The effect of non-Newtonian viscosity on the stability of the Blasius boundary layer

P T Griffiths, M T Gallagher and S O Stephen

Original citation:
Griffiths, P. T., M. T. Gallagher, and S. O. Stephen. "The effect of non-Newtonian viscosity on the stability of the Blasius boundary layer." *Physics of Fluids* 28.7 (2016): 074107.
http://dx.doi.org/10.1063/1.4958970

ISSN: 1070-6631

Publisher: AIP

The effect of non-Newtonian viscosity on the stability of the Blasius boundary layer

P. T. Griffiths,[1, a)] M. T. Gallagher,[2] and S. O. Stephen[3]

[1)] *Department of Engineering, University of Leicester, Leicester LE1 7RH, United Kingdom*

[2)] *School of Mathematics, University of Birmingham, Birmingham B15 2TT, United Kingdom*

[3)] *School of Mathematics & Statistics, The University of Sydney, NSW 2006, Australia*

We consider the stability of the non-Newtonian boundary layer flow over a flat plate. Shear-thinning and shear-thickening flows are modelled using a Carreau constitutive viscosity relationship. The boundary layer equations are solved in a self-similar fashion. A linear asymptotic stability analysis is presented in the limit of large Reynolds number. It is shown that the lower branch mode is destabilised and stabilised for shear-thinning and shear-thickening fluids, respectively. Favourable agreement is obtained between these asymptotic predictions and results owing from an equivalent Orr-Sommerfeld type analysis. Our results indicate that an increase in shear-thinning has the effect of significantly reducing the value of the critical Reynolds number, this suggests that the onset of instability will be significantly advanced in this case.

[a)] Electronic mail: paul.griffiths@le.ac.uk

I. INTRODUCTION

The stability of the boundary layer on a flat plate, often referred to as the Blasius boundary layer, in reference to the seminal work of P. R. H. Blasius[1], has been studied extensively throughout the 20^{th} century. The growth and decay of an arbitrarily small disturbance imposed upon the basic flow profile was first described by the linear stability theory introduced by Tollmien[2] and Schlichting[3]. These early works assumed that both the base flow and the disturbance were strictly parallel, that is to say that they are both only dependent on the wall normal coordinate, y^*, and not the streamwise coordinate, x^*. By imposing this parallel-flow approximation the governing perturbation equations are reduced to the familiar, more readily solvable, Orr-Sommerfeld equation. The experimental results of Schubauer and Skramstad[4] provided substantial justification for the Tollmien-Schlichting theory; with the parallel-flow results agreeing well with the experimental data.

Jordinson[5] revisited the numerical solution of the Orr-Sommerfeld equation noting a critical Reynolds number, based on a strictly parallel assumption, of 520. In an attempt to improve upon the agreement between parallel-flow theory and experimental results Barry and Ross[6] assumed a non-zero component of wall normal velocity and included some of the streamwise derivatives of the base flow, such that the governing equations remained separable. The author's modified Orr-Sommerfeld analysis revealed a slightly reduced critical Reynolds number of 500. This result did indeed provide a better agreement, in terms of the critical Reynolds number, with the detailed experimental results of Ross *et al.*[7].

Focusing on the lower branch structure of the neutral curve Smith[8] was able to include non-parallel effects using asymptotic triple-deck theory. Smith's analysis revealed that non-parallel effects are included in the calculations at $\mathcal{O}(R^{-3/4})$, where R is the Reynolds number scaled on the local boundary layer thickness. Although the analysis is based on the assumption of large Reynolds number, Smith's non-parallel results showed an improved agreement, when compared to parallel theories, with the experimental results of Ross *et al.*[7]. In an attempt to obtain equivalent non-parallel results for the upper branch of the neutral curve Bodonyi and Smith[9] consider a quintuple-deck asymptotic approach. However, unlike the lower branch analysis, the results did not provide a good agreement with experimental and Orr-Sommerfeld calculations when the Reynolds number is not large. Indeed, Healey[10] notes that this upper branch asymptotic theory is consistent only when $R > 10^5$, the ap-

proximate location at which the critical layer emerges from the viscous wall layer. Thus, when $R < 10^5$ the critical layer lies within the viscous wall layer, suggesting that, in this region, the upper-branch disturbances are instead described by a triple-deck structure. The transition from a triple-deck to a quintuple-deck structure is associated with the kink in the neutral curve. The modified triple-deck analysis of Hultgren[11] shows that both the upper and lower branches can be calculated using a single dispersion relation.

Our discussion thus far makes reference only to the class of fluids that satisfy a Newtonian governing viscosity relationship. However, there exists many physical and industrial processes where a fluids viscosity is observed to be non-constant. Fluids such as these are said to be non-Newtonian. Generalised Newtonian fluids are one of a number of classes of non-Newtonian fluids; the viscosity of a generalised Newtonian fluid is dependent solely on the shear-rate of the flow.

Previous studies that address the non-Newtonian boundary layer equations have often been concerned with generalised Newtonian fluids, and in particular fluids that satisfy a 'power-law' governing relationship, see, for example, Schowalter[12], Acrivos, Shah, and Peterson[13] and more recently Denier and Dabrowski[14]. However, when the power-law boundary layer equations are solved in a self-similar manner results for shear-thickening fluids predict a finite-width boundary layer, whilst shear-thinning results are found to decay into the far field in strongly algebraic fashion[14]. These features are associated with the inability of the power-law model to accurately describe the variation of viscosity within the boundary layer[15]. Griffiths[16] has shown, in the three-dimensional case, that steady base flow profiles obtained from a power-law formulation of the problem contrast those determined using the Carreau viscosity model. These results further question the applicability of the power-law model in high and low shear-rate environments. Indeed, linear stability analyses conducted on the rotating disk boundary layer have revealed that contradictory conclusions are reached when power-law results are compared to those owing from the Carreau fluid model[17]. These results, and the growing interesting in non-Newtonian boundary layer flows have been the motivation for the current investigation.

In this study we reconsider the problem of the boundary layer flow of a generalised Newtonian fluid using the Carreau fluid model. In addition to this we consider, for the first time, the linear stability characteristics of this flow using both asymptotic and numerical analyses. The outline of this paper is as follows. In II we derive the relevant boundary layer

equations and introduce the self-similar form of the streamwise and wall normal velocity components. In III we solve the nonlinear boundary value problem outlined in II, ensuring that the boundary layer flow matches smoothly with that of the free-stream. A linear asymptotic stability analysis is presented in IV. A new set of generalised Newtonian linear disturbance equations are derived and we present leading, and next order, results regarding the lower branch structure of the neutral stability curve. A generalised Newtonian Orr-Sommerfeld analysis is the subject matter of V. Neutral stability curves are plotted for both shear-thickening and shear-thinning fluids. In the limit of large Reynolds number our exact asymptotic results are compared to our approximate numerical solutions. Finally, in VI we discuss the results of our study and conclude by summarising our findings.

II. FORMULATION

The flow of an incompressible non-Newtonian fluid over an impermeable, semi-infinite, flat plat is governed by the continuity and Cauchy momentum equations

$$\boldsymbol{\nabla}^* \cdot \boldsymbol{u}^* = 0, \tag{1a}$$

$$\rho^* \left(\frac{\partial}{\partial t^*} + \boldsymbol{u}^* \cdot \boldsymbol{\nabla}^* \right) \boldsymbol{u}^* = -\boldsymbol{\nabla}^* p^* + \boldsymbol{\nabla}^* \cdot \boldsymbol{\tau}^*. \tag{1b}$$

Here $\boldsymbol{u}^* = (u^*, v^*)$ are the velocity components in the streamwise and wall normal coordinates (x^*, y^*), respectively. The fluid density is ρ^*, t^* is time and p^* is the fluid pressure. The stress tensor for incompressible generalised Newtonian fluids is given by

$$\boldsymbol{\tau}^* = \mu^*(\dot{\gamma}^*)\dot{\boldsymbol{\gamma}}^*,$$

where $\dot{\boldsymbol{\gamma}}^* = \boldsymbol{\nabla}^* \boldsymbol{u}^* + (\boldsymbol{\nabla}^* \boldsymbol{u}^*)^{\mathrm{T}}$ is the rate-of-strain tensor, $\mu^*(\dot{\gamma}^*)$ is the generalised Newtonian viscosity and $\dot{\gamma}^*$, the second invariant of the rate-of-strain tensor, is defined as $\dot{\gamma}^* = \sqrt{(\dot{\boldsymbol{\gamma}}^* : \dot{\boldsymbol{\gamma}}^*)/2}$. The constitutive viscosity relation considered herein is described by the Carreau [18] model

$$\mu^* = \mu^*_\infty + (\mu^*_0 - \mu^*_\infty)[1 + (\lambda^* \dot{\gamma}^*)^2]^{(n-1)/2}, \tag{2}$$

where μ^*_∞ is the infinite-shear-rate viscosity, μ^*_0 is the zero-shear-rate viscosity, λ^* is the characteristic time constant, and n is the fluid index. For $n > 1$ the fluid is said to be shear-thickening, whilst for $n < 1$ the fluid is said to be shear-thinning. The Newtonian viscosity relationship is recovered when $n = 1$.

This system is made dimensionless via the introduction of the following variables

$$(u^*, v^*) = U^*_\infty(\tilde{u}, \tilde{v}), \quad (x^*, y^*) = L^*(x, y), \quad t^* = \frac{L^*}{U^*_\infty} t, \quad p^* = \rho^*(U^*_\infty)^2 \tilde{p}, \quad \mu^* = \mu^*_0 \mu.$$

Here L^* is a typical length scale and U^*_∞ a typical free-stream speed. In order to investigate the boundary layer region close to the surface of the flat plate we rescale the problem such that

$$(\tilde{u}, \tilde{v}) = (U_B, Re^{-1/2} V_B), \quad y = Re^{-1/2} Y, \quad \tilde{p} = P_B,$$

where the Reynolds number, scaled by the zero-shear-rate, viscosity is defined as

$$Re = \frac{\rho^* U^*_\infty L^*}{\mu^*_0}.$$

At leading order, the continuity and Cauchy momentum equations (1) become

$$\frac{\partial U_B}{\partial x} + \frac{\partial V_B}{\partial Y} = 0, \tag{3a}$$

$$\frac{\partial U_B}{\partial t} + U_B\frac{\partial U_B}{\partial x} + V_B\frac{\partial U_B}{\partial Y} = -\frac{\mathrm{d}P_B}{\mathrm{d}x} + \frac{\partial}{\partial Y}\left(\mu\frac{\partial U_B}{\partial Y}\right). \tag{3b}$$

The viscosity function μ expands as such

$$\mu = \left[1 + xk^2\left(\frac{\partial U_B}{\partial Y}\right)^2\right]^{(n-1)/2}, \tag{3c}$$

where we have neglected the ratio μ^*_∞/μ^*_0 as this quantity is assumed to be small. This approximation is consistent with a number of other studies involving generalised Newtonian fluids (see, for example, Nouar, Bottaro, and Brancher[19]). The dimensionless form of the characteristic time constant is given by $k = \lambda^* U^*_\infty \sqrt{\rho^* U^*_\infty/\mu^*_0 x^*}$. We note that k is scaled by the streamwise coordinate x^*, this therefore restricts our attention to a strictly local analysis whereby k is evaluated at a specific streamwise location along the flat plate.

The system (3) is closed subject to the following boundary conditions

$$U_B = V_B = 0 \quad \text{at} \quad Y = 0, \tag{4a}$$

$$U_B \to U_e(x) \quad \text{as} \quad Y \to \infty, \tag{4b}$$

where $U_e(x)$ is the streamwise velocity component outside of the boundary layer. The first of these conditions ensures that the no-slip criterion is satisfied at the wall, the second states that the streamwise velocity inside the boundary layer must match with that of the free-stream far from the wall.

In the absence of a streamwise pressure gradient the free-stream velocity is chosen to be $U_e = 1$; thus the boundary layer equations (3) admit similarity solutions of the form

$$U_B(x, Y) = f'(\eta), \quad V_B(x, Y) = \frac{\eta f'(\eta) - f(\eta)}{2\sqrt{x}}, \tag{5}$$

where $\eta = Y/\sqrt{x}$. The function f must satisfy

$$f'''\hat{\mu} = -\frac{ff''}{2}, \tag{6a}$$

where

$$\begin{aligned}\hat{\mu} &= [1 + n(kf'')^2][1 + (kf'')^2]^{(n-3)/2} \\ &= [1 + (kf'')^2]^{(n-1)/2} + (n-1)(kf'')^2[1 + (kf'')^2]^{(n-3)/2} = \hat{\mu}_p + \hat{\mu}_s.\end{aligned} \tag{6b}$$

Here the effective viscosity function is denoted by $\hat{\mu}$. We note that the effective viscosity can be split into primary ($\hat{\mu}_p$) and secondary ($\hat{\mu}_s$) components; these functions are such that $\hat{\mu}_p|_{n=1} = 1$ and $\hat{\mu}_s|_{n=1} = 0$.

The system (6) is closed subject to the following boundary conditions

$$f = f' = 0 \quad \text{at} \quad \eta = 0, \tag{7a}$$

$$f' \to 1 \quad \text{as} \quad \eta \to \infty. \tag{7b}$$

Dabrowski [15] considered a similar problem in the case when $\mu^*_\infty/\mu^*_0 = \mathcal{O}(1)$. Our analysis is essentially a modification of his. However, owing to our formulation of the problem, we are able to make direct comparisons with the familiar Blasius solution, this proves useful in the forthcoming stability analyses.

III. BASE FLOW

Before numerically solving the nonlinear boundary-value problem defined by (6) and (7) it proves useful to first develop the large-η asymptotic form for the solution f. This ensures that the numerical solutions satisfy the correct form of asymptotic decay into the far field. Owing from (7b) we write $f = (\eta - a) + \hat{f}(\eta) + \cdots$ as $\eta \to \infty$, where a is a constant and the correction term $\hat{f}$ is such that $\hat{f} \ll 1$. By defining $\zeta = \eta - a$ and retaining only leading order terms, from (6) we have that

$$\hat{f}''' + \frac{\zeta \hat{f}''}{2} = 0,$$

where the primes denote differentiation with respect to ζ. Therefore in the limit as $\zeta \to \infty$ we find that

$$f' = 1 + A\frac{\sqrt{\pi}}{2}\operatorname{erfc}\left(\frac{\zeta}{2}\right) + \cdots = 1 + \frac{Ae^{-\zeta^2/4}}{\zeta} + \cdots,$$

where A is a constant of integration. Thus solutions owing from the Carreau fluid model exhibit the same exponential decay into the far field as the corresponding Newtonian solutions (see Jones and Watson[20]). Hence in this case the inner boundary layer flow will match smoothly with that of an outer potential flow. This is unlike the equivalent power-law analysis where the shear-thinning solutions have been shown to decay algebraically into the far field meaning that matching considerations are necessary in that case[14].

We solve (6) subject to (7a) and (7b) using a shooting method that utilises a fourth-order Runge-Kutta quadrature routine coupled with a Newton iteration scheme to determine the value of f'' at the wall. Throughout this analysis the value of k is held fixed at $k = 10$ whilst the fluid index is varied across a range of shear-thinning and shear-thickening values. Our results are presented in figures 1 and 2 and have been tabulated overleaf, with Newtonian solutions included as a comparative aid. Within Table I we provide values for the Blasius constant δ, which is given by

$$\delta = \int_0^\infty (1 - f')\,\mathrm{d}\eta = \delta^* \sqrt{\frac{\rho^* U_\infty^*}{\mu_0^* x^*}}, \tag{8}$$

where δ^* is the displacement thickness. Utilising this definition we introduce the Reynolds number $R = \rho^* U_\infty^* \delta^* / \mu_0^* = \delta\sqrt{xRe}$, based on the local boundary layer thickness. This form of the Reynolds number will be used in the forthcoming asymptotic and numerical analyses.

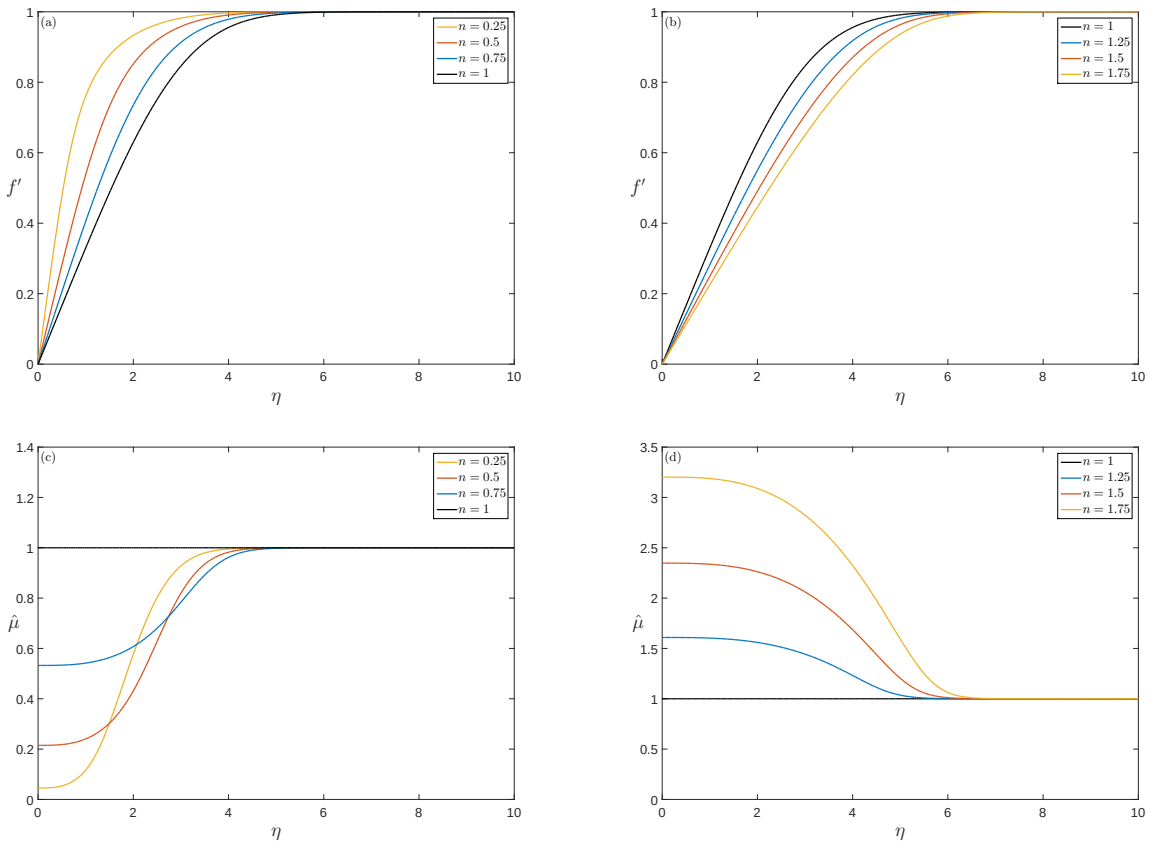

FIG. 1. Steady base flow profiles for shear-thinning and shear-thickening Carreau fluids. In (a) and (b) the streamwise velocity function f' is plotted against the boundary layer coordinate η. In (c) and (d) the effective viscosity function $\hat{\mu}$ is plotted against η. In all cases the η–axis has been truncated at $\eta = 10$. The Newtonian solutions are included as a comparative aid.

TABLE I. Numerically calculated values of the effective wall shear $f''(0)$, the effective viscosity at the wall $\hat{\mu}(0)$, and the Blasius constant δ.

n	$f''(0)$	$\hat{\mu}(0)$	δ
0.25	1.0049	0.0454	0.7391
0.5	0.5663	0.2148	1.1150
0.75	0.4117	0.5325	1.4372
1	0.3321	1	1.7208
1.25	0.2831	1.6089	1.9747
1.5	0.2498	2.3472	2.2052
1.75	0.2255	3.2020	2.4165

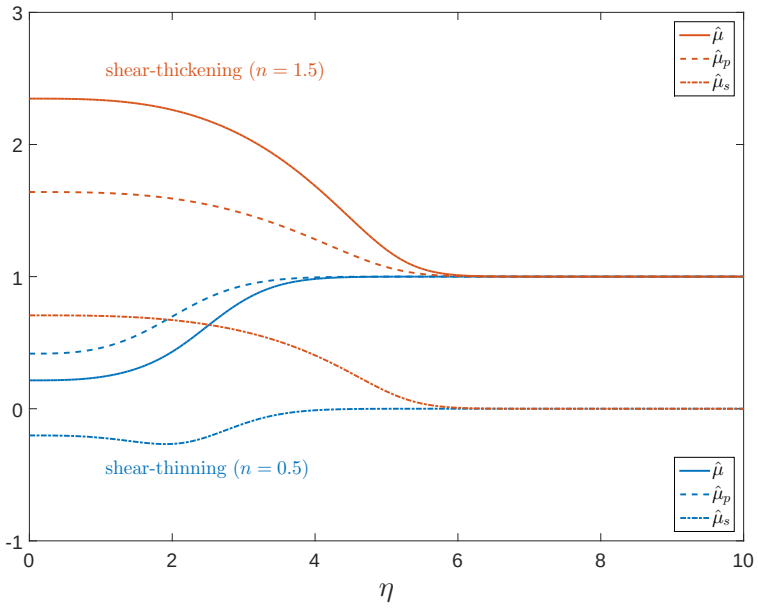

FIG. 2. The effective viscosity function $\hat{\mu}$ plotted against the boundary layer coordinate η for shear-thinning and shear-thickening Carreau fluids. As a point of reference, for both cases, the primary ($\hat{\mu}_p$) and secondary ($\hat{\mu}_s$) components of the effective viscosity function have also been included. The η–axis has been truncated at $\eta = 10$.

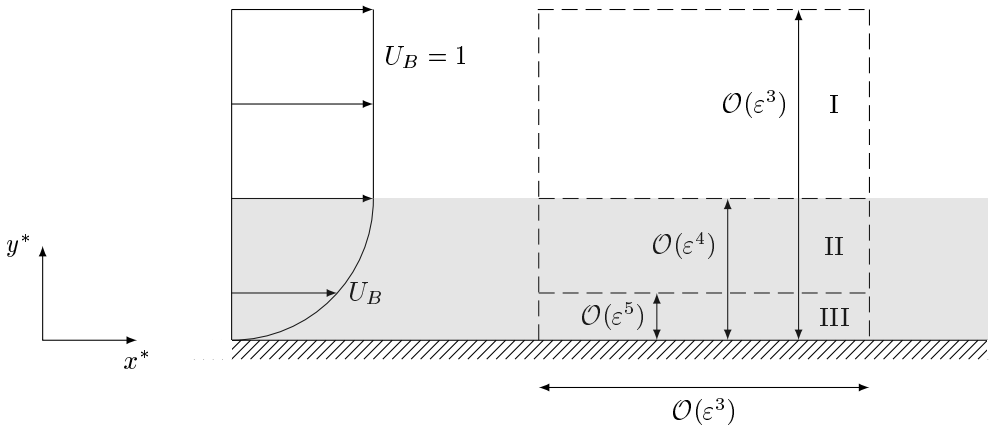

FIG. 3. Schematic diagram showing the lower branch structure of the Blasius boundary layer. The zones I, II and III denote the upper, main and lower decks respectively. The grey shaded area indicates the boundary layer region whereas the unshaded area indicates the inviscid region where the base flow matches with that of the free-stream. The small parameter ε on which the disturbance structure is based is defined in (9).

IV. ASYMPTOTIC ANALYSIS

In order to describe the lower branch structure of the neutral stability curve we assume that the Reynolds number is large. Having done so we perform a linear asymptotic stability analysis that is valid for all values of the fluid index n. As in the Newtonian case we find that on the lower branch the linear disturbances are governed by a triple-deck structure consisting of upper, main and lower decks. This is outlined schematically in Figure 3. Our small parameter, scaled on the global boundary layer thickness, is given by

$$\varepsilon = Re^{-1/8}. \tag{9}$$

The upper, main and lower decks are found to be of thickness $\mathcal{O}(\varepsilon^3)$, $\mathcal{O}(\varepsilon^4)$ and $\mathcal{O}(\varepsilon^5)$ respectively. The analysis in the upper and main decks is largely similar to that presented by Smith [8], who considered the corresponding Newtonian problem. It is within the viscous lower deck where we see the emergence of leading order generalised Newtonian terms.

We model the initial growth of the disturbances by assuming that the base flow is subject to infinitesimally small perturbations and write

$$\tilde{u} = U_0 + u(x, y, t), \quad \tilde{v} = V_0 + v(x, y, t), \quad \tilde{p} = P_0 + p(x, y, t), \tag{10}$$

where $U_0 = U_B(x,Y) + \cdots$, $V_0 = Re^{-1/2}V_B(x,Y) + \cdots$ and $P_0 = P_B(x,Y) + \cdots$, with u, v, $p = \mathcal{O}(1)$ as $\varepsilon \to 0$. After substitution of (10) into the dimensionless continuity and Cauchy momentum equations, and neglecting nonlinear terms, we arrive at the governing linear disturbance equations, namely

$$\frac{\partial u}{\partial x} + \frac{\partial v}{\partial y} = 0, \tag{11a}$$

$$\frac{\partial u}{\partial t} + U_0\frac{\partial u}{\partial x} + V_0\frac{\partial u}{\partial y} + u\frac{\partial U_0}{\partial x} + v\frac{\partial U_0}{\partial y} = -\frac{\partial p}{\partial x} + \frac{1}{Re}\left\{2\frac{\partial}{\partial x}\left(\bar{\mu}\frac{\partial u}{\partial x} + \bar{\bar{\mu}}\frac{\partial u}{\partial y}F_x^{U_0}\right) + \frac{\partial}{\partial y}\left[\bar{\mu}\left(\frac{\partial u}{\partial y} + \frac{\partial v}{\partial x}\right) + \bar{\bar{\mu}}\frac{\partial u}{\partial y}\left(1 + F_x^{V_0}\right)\right]\right\}, \tag{11b}$$

$$\frac{\partial v}{\partial t} + U_0\frac{\partial v}{\partial x} + V_0\frac{\partial v}{\partial y} + u\frac{\partial V_0}{\partial x} + v\frac{\partial V_0}{\partial y} = -\frac{\partial p}{\partial y} + \frac{1}{Re}\left\{2\frac{\partial}{\partial y}\left(\bar{\mu}\frac{\partial v}{\partial y} + \bar{\bar{\mu}}\frac{\partial u}{\partial y}F_y^{V_0}\right) + \frac{\partial}{\partial x}\left[\bar{\mu}\left(\frac{\partial u}{\partial y} + \frac{\partial v}{\partial x}\right) + \bar{\bar{\mu}}\frac{\partial u}{\partial y}\left(1 + F_x^{V_0}\right)\right]\right\}, \tag{11c}$$

where $F_z^{W_0} = (\partial W_0/\partial z)/(\partial U_0/\partial y)$ and

$$\bar{\mu} = \left[1 + \lambda^2\left(\frac{\partial U_0}{\partial y}\right)^2\right]^{(n-1)/2}, \tag{11d}$$

$$\bar{\bar{\mu}} = (n-1)\lambda^2\left(\frac{\partial U_0}{\partial y}\right)^2\left[1 + \lambda^2\left(\frac{\partial U_0}{\partial y}\right)^2\right]^{(n-3)/2}, \tag{11e}$$

with $\lambda = \lambda^* U_\infty^*/L^*$. Here $\bar{\mu}$ is the leading order viscosity function whilst $\bar{\bar{\mu}}$ is the leading order viscosity perturbation.

We expect that the lower branch mode is scaled on a streamwise length scale of $\mathcal{O}(\varepsilon^3)$. As such we consider disturbances proportional to

$$E = \exp\left\{\frac{\mathrm{i}}{\varepsilon^3}\left[\int \alpha(x,\varepsilon)\,\mathrm{d}x - \beta(\varepsilon)\tau\right]\right\},$$

where $\tau = \varepsilon t$. We restrict our attention to neutral disturbances and expand the wavenumber α, and the frequency β, as such

$$\alpha = \alpha_1 + \varepsilon\alpha_2 + \mathcal{O}(\varepsilon^2), \tag{12a}$$

$$\beta = \beta_1 + \varepsilon\beta_2 + \mathcal{O}(\varepsilon^2). \tag{12b}$$

In the subsequent analysis we adopt a multiple-scales approach whereby $\partial/\partial x$ is replaced by $\partial/\partial x + (\mathrm{i}/\varepsilon^3)\alpha$.

A. The Main Deck

The main deck encapsulates the entirety of the boundary layer therefore we reintroduce our wall normal coordinate $Y = Re^{1/2}y = \varepsilon^{-4}y = \mathcal{O}(1)$. As $Y \to 0$ we find that the base flow takes the form

$$U_0 \sim \kappa(x)Y + \mathcal{O}(Y^4), \quad V_0 \sim -\varepsilon^4\kappa'(x)Y^2/2 + \mathcal{O}(Y^5), \tag{13}$$

where $\kappa(x) = f''(0)/\sqrt{x}$. Conversely as $Y \to \infty$ the base flow is essentially that of the free-stream with $U_0 = 1$ and $V_0 = 0$. In the main deck we expand the disturbances in the form

$$u = [u_1(x,Y) + \varepsilon u_2(x,Y) + \mathcal{O}(\varepsilon^2)]E, \tag{14a}$$

$$v = [\varepsilon v_1(x,Y) + \varepsilon^2 v_2(x,Y) + \mathcal{O}(\varepsilon^3)]E, \tag{14b}$$

$$p = [\varepsilon p_1(x,Y) + \varepsilon^2 p_2(x,Y) + \mathcal{O}(\varepsilon^3)]E. \tag{14c}$$

After substitution of (14) into (11) we determine that at $\mathcal{O}(\varepsilon^{-3})$

$$u_1 = A_1(x)\frac{\partial U_B}{\partial Y}, \quad v_1 = -\mathrm{i}\alpha_1 A_1(x)U_B, \quad p_1 = p_1(x). \tag{15}$$

At the next order we have that

$$u_2 = \left[A_2(x) - A_1(x)\frac{\alpha_2}{\alpha_1}\right]\frac{\partial U_B}{\partial Y} - p_1(x)\left\{\frac{\partial}{\partial Y}\left[U_B\int_c^Y \frac{\mathrm{d}\chi}{U_B^2(x,\chi)}\right]\right\}, \tag{16a}$$

$$v_2 = -\mathrm{i}\alpha_1\left[A_2(x) - p_1(x)\int_c^Y \frac{\mathrm{d}\chi}{U_B^2(x,\chi)}\right]U_B + \mathrm{i}\beta_1 A_1(x), \tag{16b}$$

$$p_2 = p_2(x) - \alpha_1^2 A_1(x)\int_0^Y U_B^2(x,\chi)\,\mathrm{d}\chi, \tag{16c}$$

where c is a positive non-zero constant.

B. The Lower Deck

Here the wall normal coordinate is $Z = Re^{5/8}y = \varepsilon^{-5}y = \mathcal{O}(1)$, and the expansions for the disturbances are now

$$u = [U_1(x,Z) + \varepsilon U_2(x,Z) + \mathcal{O}(\varepsilon^2)]E, \tag{17a}$$

$$v = [\varepsilon^2 V_1(x,Z) + \varepsilon^3 V_2(x,Z) + \mathcal{O}(\varepsilon^4)]E, \tag{17b}$$

$$p = [\varepsilon P_1(x,Z) + \varepsilon^2 P_2(x,Z) + \mathcal{O}(\varepsilon^3)]E. \tag{17c}$$

Given (13) we write the base flow in the lower deck as such

$$U_0 = \varepsilon\kappa(x)Z + \mathcal{O}(Z^4),$$
$$V_0 = -\varepsilon^6\kappa'(x)Z^2/2 + \mathcal{O}(Z^5).$$

Substituting (17) into (11) we find that the solutions for V_i can be eliminated from the problem, at leading order we determine that

$$U_1 = B_1(x)\int_{\xi_0}^{\xi} \mathrm{Ai}(\chi)\,\mathrm{d}\chi, \tag{18a}$$
$$P_1 = -\frac{\beta_1}{\alpha_1}\frac{B_1(x)\mathrm{Ai}'(\xi_0)}{\xi_0}, \tag{18b}$$

where Ai is the decaying Airy function and

$$\xi = \left(\frac{\mathrm{i}\alpha_1\kappa}{\hat{\mu}_0}\right)^{1/3}\left(Z - \frac{\beta_1}{\alpha_1\kappa}\right).$$

For ease of notation we write $\xi_0 = \xi|_{Z=0}$, and $\hat{\mu}_0 = \hat{\mu}(0)$. At next order we find that

$$U_2 = B_2(x)\int_{\xi_0}^{\xi} \mathrm{Ai}(\chi)\,\mathrm{d}\chi + B_1(x)\frac{\alpha_2}{\alpha_1}\left\{\frac{\mathrm{Ai}''(\xi) - \mathrm{Ai}''(\xi_0)}{3} + \zeta_0[\mathrm{Ai}(\xi) - \mathrm{Ai}(\xi_0)]\right\}, \tag{19a}$$
$$P_2 = -\frac{\beta_1}{\alpha_1}\left\{\frac{B_2(x)\mathrm{Ai}'(\xi_0)}{\xi_0} + \frac{B_1(x)}{\xi_0}\frac{\alpha_2}{\alpha_1}\left[\frac{\mathrm{Ai}''''(\xi_0)}{3} + \zeta_0\mathrm{Ai}''(\xi_0) - \mathrm{Ai}'(\xi_0)\right]\right\}, \tag{19b}$$

where $\zeta_0 = \xi_0[(\alpha_1\beta_2/\beta_1\alpha_2) - 1]$.

C. The Upper Deck

We introduce the upper deck wall normal coordinate as $\bar{y} = Re^{3/8}y = \varepsilon^{-3}y = \mathcal{O}(1)$, and write the disturbance expansions as

$$u = [\varepsilon\bar{u}_1(x,\bar{y}) + \varepsilon^2\bar{u}_2(x,\bar{y}) + \mathcal{O}(\varepsilon^3)]E, \tag{20a}$$
$$v = [\varepsilon\bar{v}_1(x,\bar{y}) + \varepsilon^2\bar{v}_2(x,\bar{y}) + \mathcal{O}(\varepsilon^3)]E, \tag{20b}$$
$$p = [\varepsilon\bar{p}_1(x,\bar{y}) + \varepsilon^2\bar{p}_2(x,\bar{y}) + \mathcal{O}(\varepsilon^3)]E. \tag{20c}$$

In the upper deck we have that $U_0 = 1$ and $V_0 = 0$. Substituting (20) into (11), and after elimination of the velocity components, we find that the solutions in the upper deck, at the first two orders, are governed by the following pressure equations

$$\bar{p}_1 = C_1(x)e^{-\alpha_1\bar{y}}, \quad \bar{p}_2 = [C_2(x) - \alpha_2 C_1(x)\bar{y}]e^{-\alpha_1\bar{y}}. \tag{21}$$

Utilising these expressions for $\bar{p}_1$ and $\bar{p}_2$ we determine that

$$\bar{v}_1 = -\mathrm{i}e^{-\alpha_1\bar{y}}C_1(x), \quad \bar{v}_2 = -\mathrm{i}e^{-\alpha_1\bar{y}}\left[C_2(x) + C_1(x)\left(\frac{\beta_1}{\alpha_1} - \alpha_2\bar{y}\right)\right]. \tag{22}$$

Solutions for $\bar{u}_i$ are not stated here as these are superfluous to the remaining analysis.

D. Matching

In order to determine governing eigenrelations for the wavenumbers α_1 and α_2 we match our solutions between the three decks with the aim of eliminating the unknown functions of x.

Matching the solutions for v between the main and upper decks gives

$$P_1(x) = \alpha_1 A_1(x), \tag{23a}$$

$$P_2(x) = \alpha_1 A_2(x) - 2\beta_1 A_1(x) + \alpha_1^2 A_1(x)\left[\int_0^\infty U_B^2(x,\chi)\,\mathrm{d}\chi - \int_c^\infty \frac{\mathrm{d}\chi}{U_B^2(x,\chi)}\right]. \tag{23b}$$

Similarly, matching the solutions for u between the lower and main decks gives

$$B_1(x)\int_{\xi_0}^\infty \mathrm{Ai}(\xi)\,\mathrm{d}\xi = \kappa A_1(x), \tag{24a}$$

$$\begin{aligned} B_2(x)\int_{\xi_0}^\infty \mathrm{Ai}(\xi)\,\mathrm{d}\xi = \kappa A_2(x) + B_1(x)\frac{\alpha_2}{\alpha_1}\left[\frac{\mathrm{Ai}''(\xi_0)}{3} + \zeta_0\mathrm{Ai}(\xi_0)\right] \\ - \kappa\left[A_1(x)\frac{\alpha_2}{\alpha_1} + \alpha_1 A_1(x)\int_c^0 \frac{\mathrm{d}\chi}{U_B^2(x,\chi)}\right]. \end{aligned} \tag{24b}$$

Combining (18b), (23a) and (24a) we eliminate $A_1(x)$ and $B_1(x)$ and obtain our leading order eigenrelation

$$\frac{\mathrm{Ai}'(\xi_0)}{\int_{\xi_0}^\infty \mathrm{Ai}(\xi)\,\mathrm{d}\xi} = \frac{\alpha_1}{\kappa^2}\left(\frac{\mathrm{i}\alpha_1\kappa}{\hat{\mu}_0}\right)^{1/3}. \tag{25}$$

Combining (19b), (23b) and (24b) we eliminate $A_2(x)$ and $B_2(x)$ and obtain the eigenrelation at the next order. Having restricted our attention to neutral disturbances we require that α_i must be real. In order for α_1 to be real we require that $\xi_0 = -2.2970\mathrm{i}^{1/3}$, thus

$$\frac{\mathrm{Ai}'(\xi_0)}{\int_{\xi_0}^\infty \mathrm{Ai}(\xi)\,\mathrm{d}\xi} = 1.0003\mathrm{i}^{1/3}, \tag{26}$$

and (25) yields

$$\alpha_1 = 1.0002\sqrt[4]{\hat{\mu}_0}[f''(0)]^{5/4}x^{-5/8}, \tag{27a}$$

$$\beta_1 = 2.2973\sqrt{\hat{\mu}_0}[f''(0)]^{3/2}x^{-3/4}. \tag{27b}$$

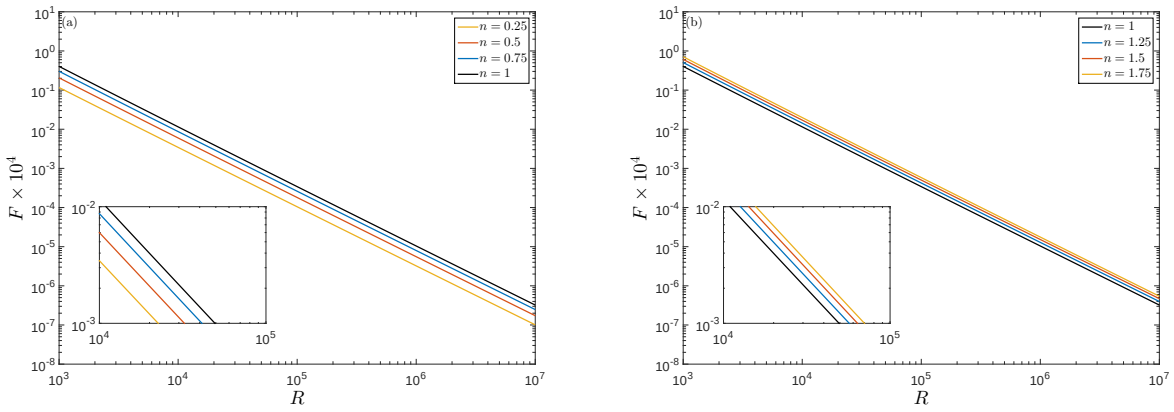

FIG. 4. Asymptotic predictions of the neutrally stable lower branch mode for (a) shear-thinning and (b) shear-thickening Carreau fluids. Using a log–log scale the experimental frequency parameter is plotted against the Reynolds number based on the local boundary layer thickness.

In order for α_2 to be real we determine that

$$\beta_2 = \frac{\beta_1^2}{\alpha_1} + \frac{\alpha_1\beta_1}{2}\hat{I}, \quad \text{where} \quad \hat{I} = \sqrt{x}\int_0^\infty (f')^{-2} - (f')^2 \,\mathrm{d}\eta = \sqrt{x}\tilde{I}. \tag{28}$$

Details regarding the evaluation of the singular integral $\tilde{I}$ are outlined in the Appendix A. Having computed $\tilde{I}$ we are able to determine similar expressions for α_2 and β_2. However, at this stage, it proves more useful to interpret our results in terms of the experimental frequency parameter $F = \omega^*\mu_0^*/\rho^*(U_\infty^*)^2 = Re^{-3/4}\beta$. Theoretical predictions are often presented in the (R, F) plane as it easier to make direct comparisons with experimental results. Despite the lack of experimental data for the cases when $n \neq 1$ we choose to present our results in a manner that is consistent with previous investigations.

Given the definitions of R, F, and our results for β_1 and β_2 ((27b) and (28)), we have that

$$F = 2.2973\sqrt{\hat{\mu}_0}[\delta f''(0)]^{3/2}R^{-3/2}\{1+2.2968[\hat{\mu}_0\delta f''(0)]^{1/4}[1+0.2177 f''(0)\tilde{I}]R^{-1/4}+\cdots\}. \tag{29}$$

This expression represents two terms in the asymptotic expansion of the neutrally stable lower branch mode. The dependence of the result on the fluid index n is encompassed in the factors of $\hat{\mu}_0$, δ, $f''(0)$ and $\tilde{I}$ appearing in (29). Plots of F against R for a range of shear-thinning and shear-thickening values are presented in Figure 4. The flow is unstable in the region above the curves. Thus, as n decreases our results predict that the lower branch

mode of the neutral curve will become less stable. Furthermore, observations made from Figure 4 suggest that the flow will be significantly less stable as the fluid index is decreased from unity, whilst for values of n larger than 1 the flow will become only marginally more stable. However, the stabilising or destabilising effect of the fluid index n in terms of the critical Reynolds number can only be determined via numerical calculations of the neutral stability curve.

Interestingly, in the lower deck, we find that terms owing from the derivatives of the viscosity functions do not appear in the calculations until the fifth order ($\mathcal{O}(R^{-3/4})$), the same order at which non-parallel effects are first encountered. This suggests that these additional viscous effects will not provide a significant contribution to the linear stability characteristics of the boundary layer flow when a parallel flow assumption is imposed. It is also noteworthy to mention that terms owing from both the leading order and perturbed viscosity functions appear in the calculations, at this order, in the main deck. This suggests that the non-parallel stability of the flow may be more significantly affected by a non-Newtonian rheology.

V. NUMERICAL ANALYSIS

In order to compliment the asymptotic results obtained previously we introduce a comparable Orr-Sommerfeld-type analysis. By assuming that both the base flow and the disturbances are strictly parallel, and that the disturbances have the normal mode form:

$$u(x,y,t) = \hat{u}(y)e^{\mathrm{i}(\alpha x-\beta t)}, \tag{30a}$$

$$v(x,y,t) = \hat{v}(y)e^{\mathrm{i}(\alpha x-\beta t)}, \tag{30b}$$

$$p(x,y,t) = \hat{p}(y)e^{\mathrm{i}(\alpha x-\beta t)}, \tag{30c}$$

the governing linear disturbance equations (11) are reduced to a set of ordinary differential equations. Eliminating the streamwise velocity and pressure perturbations we determine a generalised Newtonian Orr-Sommerfeld equation

$$\begin{aligned}\tilde{\mu}(\hat{v}'''' - 2\alpha^2\hat{v}'' + \alpha^4\hat{v}) + 2\tilde{\mu}'(\hat{v}''' - \alpha^2\hat{v}') + \tilde{\mu}''(\hat{v}'' + \alpha^2\hat{v}) \\ + \tilde{\tilde{\mu}}(\hat{v}'''' + \alpha^2\hat{v}'') + 2\tilde{\tilde{\mu}}'\hat{v}''' + \tilde{\tilde{\mu}}''\hat{v}'' = \mathrm{i}R[(\alpha U_0 - \beta)(\hat{v}'' - \alpha^2\hat{v}) - \alpha U_0''\hat{v}].\end{aligned} \tag{31a}$$

Here the primes denote differentiation with respect to y and

$$\tilde{\mu} = [1 + (\lambda U_0')^2]^{(n-1)/2} = [1 + (kf'')^2]^{(n-1)/2} = \hat{\mu}_p, \tag{31b}$$

$$\tilde{\tilde{\mu}} = (n-1)(\lambda U_0')^2[1 + (\lambda U_0')^2]^{(n-3)/2} = (n-1)(kf'')^2[1 + (kf'')^2]^{(n-3)/2} = \hat{\mu}_s. \tag{31c}$$

We note that $\mathrm{d}^i U_0/\mathrm{d}y^i = \delta^i(\mathrm{d}^{i+1}f/\mathrm{d}\eta^{i+1})$, with δ as given in (8), and that substitution of $n = 1$ returns the familiar Newtonian Orr-Sommerfeld equation, as would be expected.

We solve the eigenvalue problem (31) subject to the boundary conditions

$$\hat{v} = \hat{v}' = 0 \quad \text{at} \quad y = 0, \tag{32a}$$

$$\hat{v} \to \hat{v}' \to 0 \quad \text{as} \quad y \to \infty. \tag{32b}$$

The neutral temporal and spatial stability of the system is determined using Chebfun[21], more specifically the `eigs` routine developed by Driscoll, Bornemann, and Trefethen[22]. By restricting α to be real, and by fixing values for α and R, the eigenvalue problem for β is solved subject to (32). The most dangerous eigenvalue, that with largest imaginary part, is calculated. We then use a bisection algorithm to find, for a fixed R, the value of α corresponding to $\beta_\mathrm{i} = 0$. The curves of neutral spatial stability are then determined from

the eigenvalues with zero imaginary part, in which case $\beta = \beta_{\mathrm{r}}$. Particular attention has been paid to the location of the critical Reynolds number R_c, and the corresponding critical values of the wavenumber α_c, and frequency β_c. The results for these critical values, for a range of the fluid index n, are displayed in Table II.

In order to validate our numerical scheme we compare the results for $n = 1$ with those of Thomas[23] who considered the corresponding Newtonian problem. As noted in Table II our Newtonian values for R_c, α_c and β_c are in excellent agreement with Thomas[23]. We contribute any marginal differences, between the quoted critical values, to the extremely high accuracy of the Chebfun software[21].

Results from our numerical computations are presented in figures 5, 6 and 7. In Figure 5 we plot, for moderate Reynolds numbers, the curves of neutral temporal and spatial stability for shear-thinning and shear-thickening Carreau fluids. We observe that the critical Reynolds number increases with the fluid index n and does so in a linear fashion. This suggests that, in terms of the critical Reynolds number, shear-thinning has the effect of destabilising the boundary layer flow whilst shear-thickening appears to have the opposite effect. In agreement with the asymptotic predictions, we find that the lower branch mode is destabilised and stabilised for flows with $n < 1$ and $n > 1$, respectively. However, interestingly, we note that the stability characteristics of the upper branch mode does not mirror that of the lower branch. The upper branch is in fact stabilised for shear-thinning fluids and destabilised for shear-thickening fluids. Our predictions suggest that the upper branch of the neutral stability curve is more noticeably affected by the introduction of a non-Newtonian rheology.

We plot a comparison between our numerical predictions and our exact asymptotic solutions in Figure 6. Using a logarithmic scale the frequency parameter F is plotted against the Reynolds number R. An excellent quantitative agreement is observed between the two sets of solutions, especially in the limit of large Reynolds number. For clarity of presentation we choose to plot only one shear-thinning and one shear-thickening profile. However, we note that an equally good agreement is observed for each n in the region of interest.

In order to investigate the effect the derivatives of the viscosity functions have on the linear stability characteristics of the flow we remove the $\tilde{\mu}'$, $\tilde{\mu}''$, $\tilde{\tilde{\mu}}'$, and $\tilde{\tilde{\mu}}''$ terms from (31a) and recompute the curves of neutral stability. These results, for both shear-thinning and shear-thickening fluids, are presented in Figure 7. As predicted by the asymptotic theory, these additional, higher order viscous effects do not significantly alter the linear stability

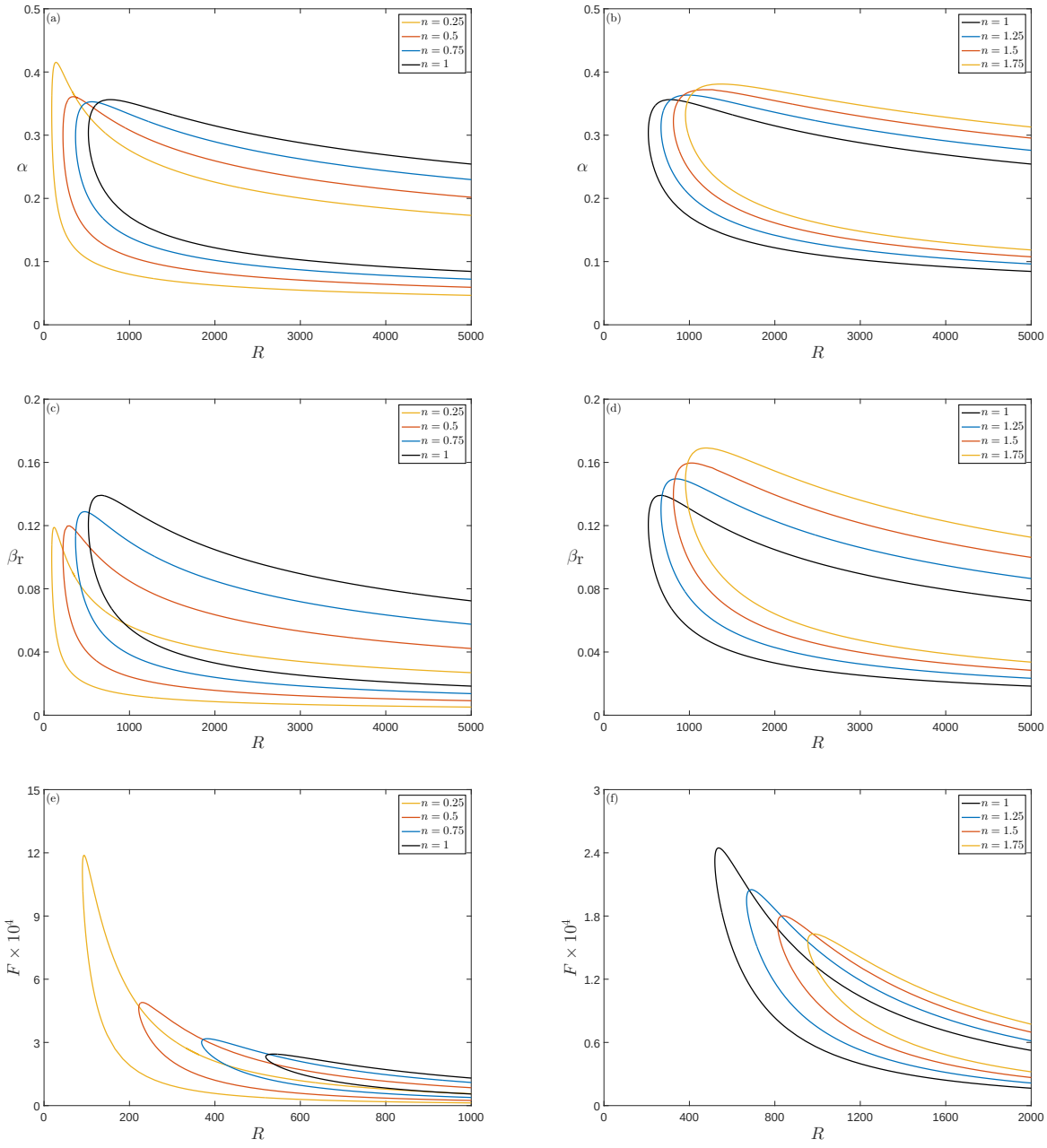

FIG. 5. Curves of neutral stability for (a), (c) and (e) shear-thinning and (b), (d) and (f) shear-thickening Carreau fluids. In (a) and (b), (c) and (d) and (e) and (f) we plot the wavenumber, real part of the frequency and the experimental frequency parameter against R, respectively. In all cases the R–axis has been truncated at $R = 5000$. The Newtonian solutions are included as a comparative aid.

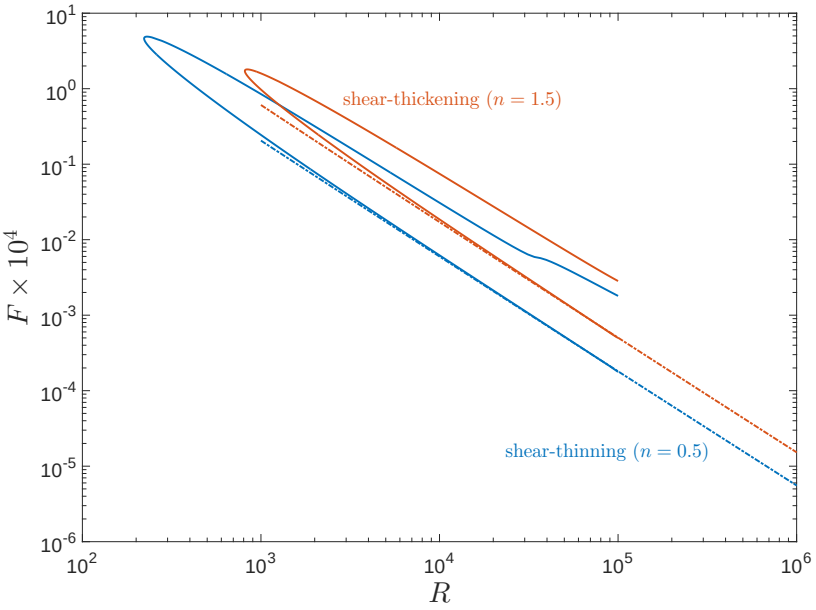

FIG. 6. Large Reynolds number neutral stability curves presented in the R–F plane for shear-thinning and shear-thickening Carreau fluids. The dashed lines represent the two term asymptotic solutions determined in IV. The numerical solutions have been truncated at $R = 10^5$.

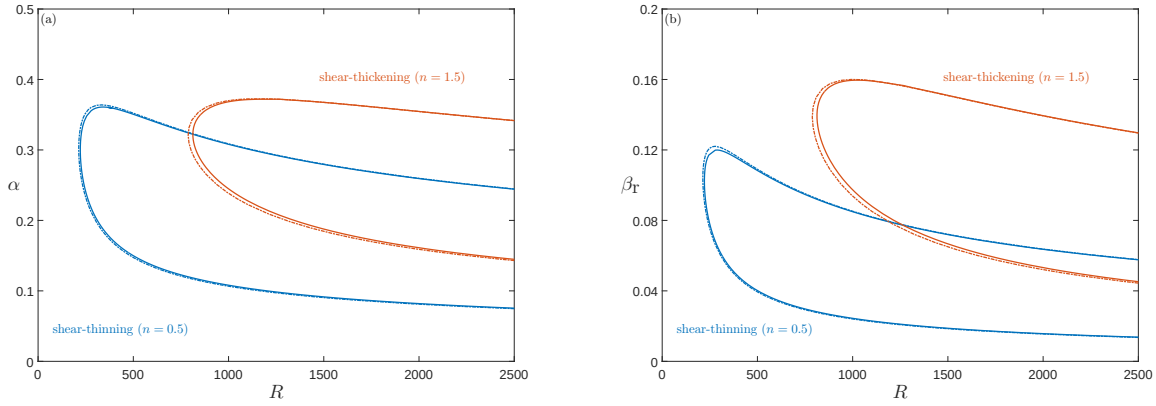

FIG. 7. A comparison between shear-thinning and shear-thickening neutral stability curves presented in the (R, α) and (R, β_r) planes. The solid lines are a reproduction of the curves plotted in Figure 5. The dashed lines represent an Orr-Sommerfeld solution where the derivatives of the viscosity functions have been ignored. In both cases the R–axis has been truncated at $R = 2500$.

TABLE II. Numerically calculated values of the critical Reynolds number R_c and the corresponding critical eigenvalues. Our Newtonian solutions are excellent in agreement with those of Thomas[23] who notes that $R_c = 519.2$, $\alpha_c = 0.303$ and $\beta_c = 0.120$.

n	R_c	α_c	β_c
0.25	89.82	0.3375	0.0997
0.5	221.69	0.2977	0.1013
0.75	368.83	0.2977	0.1108
1	519.12	0.3022	0.1198
1.25	667.58	0.3122	0.1300
1.5	812.61	0.3212	0.1390
1.75	953.52	0.3307	0.1478

characteristics, under the assumption of parallel flow.

VI. DISCUSSION AND CONCLUSIONS

In this study we have considered the problem of the boundary layer flow of a generalised Newtonian fluid with constitutive viscosity relationship governed by a modified Carreau model. Our base flow solutions are such that far from the flat plate, at the outer edge of the boundary layer, a Newtonian viscosity relationship is recovered. It would be expected that the boundary layer thickness decreases and increases for shear-thinning and shear-thickening fluids respectively. This intuition is confirmed by the self-similar velocity profiles displayed in Figure 1.

The triple-deck, asymptotic linear stability analysis presented in IV assumes that, irrespective of the fluid index n, the lower-branch mode is scaled on a streamwise length scale of $\mathcal{O}(R^{-3/4})$. It is within the viscous lower deck where we see the emergence of leading order non-Newtonian correction terms. Our analysis reveals that the structure of the lower branch neutral mode is affected by the effective viscosity at the wall, the effective wall shear and the dimensionless thickness of the boundary layer. Results owing from our two term asymptotic expression (29) show that the lower branch mode will be destabilised and stabilised for shear-thinning and shear-thickening fluids, respectively. We demonstrate that a two term asymptotic expansion is sufficient to give suitable agreement, in the limit of large Reynolds number, with parallel flow results owing from an Orr-Sommerfeld type analysis. However, the asymptotic framework presented here has the capacity to take non-parallel flow effects into account. We note that non-parallel terms first appear in the calculations at the fifth order for both Newtonian[8] and non-Newtonian flows. It transpires that additional viscous terms owing from the derivatives of the two viscosity functions ($\bar{\mu}$ and $\bar{\bar{\mu}}$, given in (11)) also enter the calculations at this order. This suggests that an extension of the current asymptotic analysis, to include non-parallel effects, certainly warrants future investigation.

In V we derived a new, generalised Newtonian, Orr-Sommerfeld equation that takes into account both primary and secondary viscous effects. Our numerical results help to support our asymptotic hypotheses and we find that the lower branch mode is indeed destabilised and stabilised for shear-thinning and shear-thickening fluids, respectively. This destabilising/stabilising nature is reaffirmed by our predictions for the onset of linear instability. We find there is a near perfect linear relationship between the value of the fluid index n, and the critical Reynolds number R_c, see Figure 8. Interestingly, we note that in the cases when the

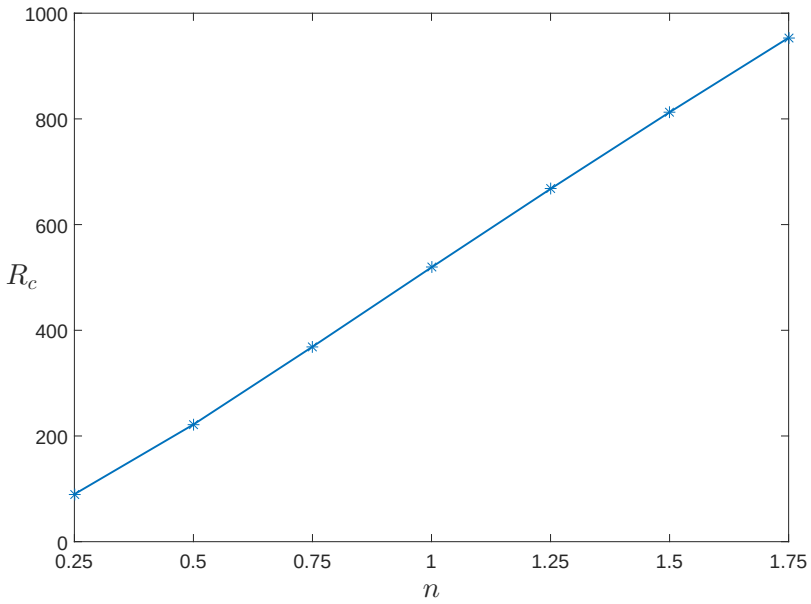

FIG. 8. Variation of the critical Reynolds number R_c, with the fluid index n, for fluids with a constitutive viscosity relationship governed by a modified Carreau model.

lower branch mode is destabilised, the upper branch is stabilised and vice-versa. Our large Reynolds number solutions reveal that for all values of the fluid index the familiar kink in the upper branch mode, associated with location at which the critical layer emerges from the viscous wall layer, is always apparent. This can be observed in Figure 6 for the case when $n = 0.5$. Due to the truncation of the numerical solutions this is not observed when $n = 1.5$ as, in this case, the transition occurs at a value of the Reynolds number greater than $R = 10^5$. The asymptotic prediction that terms associated with the derivatives of the viscosity functions have a minimal affect on the linear stability characteristics of the parallel flow has been readily verified by our Orr-Sommerfeld analysis. For brevity we have chosen to investigate only the case when $k = 10$. However, additional computations performed with $k = 1$ and $k = 100$ reveal that reducing the value of the dimensionless equivalent of the characteristic time constant has the effect of dampening any shear-thinning or shear-thickening effects, whilst increasing the value of k serves to enhance these effects.

In conclusion, we have demonstrated that the boundary layer flow of a generalised Newtonian fluid over an impermeable, semi-infinite, flat plate is amenable to both asymptotic and numerical linear stability analyses. Our results suggest that the onset of instability is

advanced for shear-thinning fluids whilst it is delayed for shear-thickening fluids. These findings are consistent with those of Lashgari *et al.*[24] who considered the instability of the flow past a circular cylinder using the Carreau fluid model scaled by the zero-shear-rate viscosity. The author's conclude that it is indeed the effect of shear-thinning that is destabilising, noting that shear-thickening effects serve to dramatically stabilise the circular cylinder flow. Although the geometry and base flow associated with the aforementioned problem are clearly very different to this investigation, the results do go some way in supporting our claims.

In addition to extending the current asymptotic analysis to include non-parallel and higher-order viscous effects there are a number of other natural extensions of this study. Firstly, the upper branch mode could be investigated asymptotically. It would be of particular interest to see how our large Reynolds number numerical predictions compare to an equivalent, exact, analytic description of the upper branch neutral mode. The Newtonian studies of Bodonyi and Smith[9] and Hultgren[11] may provide a useful basis for the development a generalised Newtonian investigation such as this. Secondly, in an attempt to validate our theoretical predictions, it would be advantageous to determine experimental results for a range of the fluid index n. It must be stated that in the absence of any experimental validation the results presented in this study must be considered as theoretical predictions only. To the best of the author's knowledge no such experiments have yet taken place, suggesting that this is an area that requires future investigation.

TABLE III. Numerically calculated values of the singular integral $\tilde{I}$.

n	$\tilde{I}$
0.25	-0.0357
0.5	-1.0714
0.75	-1.9863
1	-2.7950
1.25	-3.5171
1.5	-4.1692
1.75	-4.7641

ACKNOWLEDGMENTS

Parts of this work were completed whilst P. T. G. was visiting the School of Mathematics and Statistics at the University of Sydney. Their financial support is gratefully acknowledged.

Appendix A: The Singular Integral $\tilde{I}$

As noted in IV the result for β_2 is dependent on the singular integral $\tilde{I}$, defined as such

$$\tilde{I} = \int_0^\infty (f')^{-2} - (f')^2 \, \mathrm{d}\eta.$$

We find that for each n in the region of interest $\tilde{I}$ is singular at the point $\eta = 0$. Therefore, following Smith[8], we choose to numerically compute only the (Hadamard) finite part of the integral. The Newtonian study of Bodonyi and Smith[9] quote a value for $\tilde{I}$ of -2.7950. We return exactly the same result for the case when $n = 1$. Corresponding results for the cases when $n \neq 1$ are tabulated above.

In order to numerically compute $\tilde{I}$ we first expand the function $f'(\eta)$ about the point $\eta = 0$, this yields

$$f'(\eta) = f''(0)\eta - \frac{[f''(0)]^2\eta^4}{48\hat{\mu}_0} + \frac{3[f''(0)]^2\hat{\mu}_0'\eta^5}{240\hat{\mu}_0^2} + \mathcal{O}(\eta^6) \quad \text{as} \quad \eta \to 0.$$

Therefore

$$(f')^{-2} - (f')^2 = \frac{1}{[f''(0)]^2\eta^2} + \frac{\eta}{24f''(0)\hat{\mu}_0} - \frac{\hat{\mu}_0'\eta^2}{40f''(0)\hat{\mu}_0^2} - [f''(0)]^2\eta^2 + \mathcal{O}(\eta^3) \quad \text{as} \quad \eta \to 0.$$

Thus for some positive non-zero constant c we have that

$$\begin{aligned}\tilde{I} &= \int_0^\infty (f')^{-2} - (f')^2 \,\mathrm{d}\eta \\ &= \int_0^c \frac{1}{[f''(0)]^2\eta^2} + \frac{\eta}{24 f''(0)\hat{\mu}_0} - \frac{\hat{\mu}_0'\eta^2}{40 f''(0)\hat{\mu}_0^2} - [f''(0)]^2\eta^2 + \mathcal{O}(\eta^3)\,\mathrm{d}\eta \\ &+ \int_c^\infty (f')^{-2} - (f')^2 \,\mathrm{d}\eta = \tilde{I}_1 + \tilde{I}_2.\end{aligned}$$

We calculate $\tilde{I}_1$ analytically using Hadamard regularisation, whilst $\tilde{I}_2$ is computed numerically. For each n the value of c is chosen such that suitably converged solutions are achieved.

REFERENCES

[1] H. Blasius, "Grenzschichten in Flüssigkeiten mit kleiner Reibung," Z. Math. Phys. **56**, 1–37 (1908).

[2] W. Tollmien, "Über die Entstehung der Turbulenz," Nachr. Ges. Wiss. Göttingen Math.-Phys. Kl. **II**, 21–44 (1929).

[3] H. Schlichting, "Laminare strahlausbreitung," Z. Angew. Math. Mech. **13**, 260–263 (1933).

[4] G. B. Schubauer and H. K. Skramstad, "Laminar Boundary-Layer Oscillations and Transition on a Flat Plate," J. Res. Nat. Bur. Stand. **38**, 251–292 (1947).

[5] R. Jordinson, "The flat plate boundary layer. Part 1. Numerical integration of the Orr-Sommerfeld equation," J. Fluid Mech. **43**, 801–811 (1970).

[6] M. D. J. Barry and M. A. S. Ross, "The flat plate boundary layer. Part 2. The effect of increasing thickness on stability," J. Fluid Mech. **43**, 813–818 (1970).

[7] J. A. Ross, F. H. Barnes, J. G. Burns, and M. A. S. Ross, "The flat plate boundary layer. Part 3. Comparison of theory with experiment," J. Fluid Mech. **43**, 819–832 (1970).

[8] F. T. Smith, "On the non-parallel flow stability of the Blasius boundary layer," Proc. R. Soc. Lond. A **366**, 91–109 (1979).

[9] R. J. Bodonyi and F. T. Smith, "The upper branch stability of the Blasius boundary layer, including non-parallel flow effects," Proc. R. Soc. Lond. A **375**, 65–92 (1981).

[10] J. J. Healey, "On the neutral curve of the flat-plate boundary layer: comparison between experiment, Orr-Sommerfeld theory and asymptotic theory," J. Fluid Mech. **288**, 59–73 (1995).

[11]L. S. Hultgren, "Higher eigenmodes in the Blasius boundary-layer stability problem," Phys. Fluids **29**, 2947–2951 (1987).

[12]W. R. Schowalter, "The application of boundary-layer theory to power-law pseudoplastic fluids: similar solutions," AIChE J. **6**, 24–X28 (1960).

[13]A. Acrivos, M. J. Shah, and E. E. Peterson, "Momentum and heat transfer in laminar boundary-layer flows of non-Newtonian fluids past external bodies," AIChE J. **6**, 312–317 (1960).

[14]J. P. Denier and P. P. Dabrowski, "On the boundary-layer equations for power-law fluids," Proc. R. Soc. Lond. A **460**, 3143–3158 (2004).

[15]P. P. Dabrowski, *Boundary-layer Flows in Non-Newtonian Fluids*, Ph.D. thesis, School of Mathematical Sciences, The University of Adelaide (2009).

[16]P. T. Griffiths, "Flow of a generalised newtonian fluid due to a rotating disk," J. Non-Newtonian Fluid Mech. **221**, 9–17 (2015).

[17]P. T. Griffiths, *Hydrodynamic Stability of Non-Newtonian Rotating Boundary-Layer Flows*, Ph.D. thesis, School of Mathematics, University of Birmingham (2015).

[18]P. J. Carreau, "Rheological Equations from Molecular Network Theories," Trans. Soc. Rheolo. **16:1**, 99–127 (1972).

[19]C. Nouar, A. Bottaro, and J. P. Brancher, "Delaying transition to turbulence in channel flow: revisiting the stability of shear-thinning fluids," J. Fluid Mech. **592**, 177–194 (2007).

[20]C. W. Jones and R. J. Watson, "Laminar Boundary Layers," (Oxford University Press, 1963) Chap. V, pp. 222–226.

[21]T. A. Driscoll, N. Hale, and L. N. Trefethen, *Chebfun Guide* (Pafnuty Publications, 2014).

[22]T. A. Driscoll, F. Bornemann, and L. N. Trefethen, "The chebop system for automatic solution of differential equations," BIT Numer. Math. **48**, 701–723 (2008).

[23]C. Thomas, *Numerical Simulations of Disturbance Development in Rotating Boundary-Layers*, Ph.D. thesis, School of Mathematics, Cardiff University (2007).

[24]I. Lashgari, J. O. Pralits, F. Giannetti, and L. Brandt, "First instability of the flow of shear-thinning and shear-thickening fluids past a circular cylinder," J. Fluid Mech. **701**, 201–227 (2012).